Asymmetrical Molecular Aggregation in Spherulitic Dye Films

Jian Tao, Guangzhao Mao,* and Lars Daehne*

Contribution from the Department of Chemical Engineering and Materials Science, Wayne State University, 5050 Anthony Wayne Drive, Detroit, Michigan 48202

Received November 5, 1998

Abstract: A recently developed method of spherulitic crystallization was used for the preparation of highly ordered 80 nm thin films of the dye 1.7-bis(dimethylamino)heptamethinium perchlorate ($BDH^+ClO_4^-$). Depending on the crystallization temperature, the film color and surface topography varied widely, while the crystal structure and film thickness remained the same. At low undercooling, two homogeneous regions were obtained. One showed in-plane symmetrical and the other asymmetrical growth behaviors. At high undercooling, a banded spherulitic structure with rainbow-like colors developed, whose formation is attributed to the out-of-plane asymmetrical growth. The spherulitic growth kinetics, microstructure, and optical properties were investigated by optical microscopy, atomic force, and scanning tunneling microscopy in static and real time mode. A molecular mechanism is proposed which originates from different directions of macroscopic growth and microscopic molecular attachment dictated by the three-dimensional crystal lattice. This mechanism is consistent with the optical spectra and surface topography observed. This mechanism explains the exposure of different crystal faces, asymmetrical molecular attachment, fluctuation in growth rate, film thickness, and viscosity in the amorphous phase. Understanding the molecular origins of J-aggregation in thin dye films allows one to control and manipulate the film color almost in the whole visible wavelength range.

Introduction

Besides their historical function in paint formulation, dyes are used today in many optical signal recording processes such as photography, xerography, laser printing, and write-once-read-many-times (WORM) memory systems.[1] Furthermore, organic dye thin films have found a wide range of high technology applications, which include dichroic color filters for liquid crystal displays, field effect transistors for optoelectronic switches, solar photovoltaic cells, and organic light emitting diodes (OLEDs).[2] Most of the dye functions are based on collective properties, such as photoconductivity,[3] coherent energy transfer,[4] spectral sensitization of semiconductors,[5] and specific absorption or reflection properties.[6] These properties are determined primarily by the interactions between the dye molecules, and vary significantly with their separation, mutual orientation, and inclination with respect to the substrate.[7] These structural factors are sometimes categorically referred to as the supramolecular architecture.[8] Despite its importance, the supramolecular architecture can hardly be controlled in three-dimensions (3-D) by the known film deposition methods, such as vacuum deposition, epitaxy, self-assembly, Langmuir−Blodgett deposition, and spin coating.[9] Recently, a new method called the Thin Layer Aggregation (TLA) was developed, by which highly ordered 80 nm films of the model polymethine dye 1.7-bis(dimethylamino)heptamethine (BDH^+) with large regions of unique molecular orientations can be prepared.[10] The method is based on the spherulitic crystallization of undercooled amorphous films of dye salts. It enables the variation of not only the crystalline lattice orientation[11] but also the crystalline lattice structure itself.[10] By using different aggregation temperatures, a surprisingly broad range of color was obtained for the same crystal structure. In addition, unusual growth phenomena were observed, including the periodic variation in film color or banded growth, the curved or bent growth, and the formation of long-range patterns.[12] Spectroscopic investigations have yielded important clues to the supramolecular architecture of the film, yet there is no satisfactory explanation of the spherulitic growth process at the molecular level.[11] The high degree of color and structural variation affects reproducibility and prevents large-scale orientation of the aggregates. To control the growth pattern and to tune the optical properties of dye thin films, we studied the mechanism of spherulitic crystallization by spectroscopic methods, kinetic investigations, static and real time atomic force microscopy (AFM), and high-resolution scanning tunneling microscopy (STM). The unique and specific structure and color correlation of $BDH^+ClO_4^-$ thin films allowed us to draw conclusions concerning the supramolecular architecture

(1) Zollinger, H. *Color Chemistry: Syntheses, Properties, and Applications of Organic Dyes and Pigments*; VCH: New York, 1987. Keller, K., Ed. *Science and Technology of Photography*; VCH: Weinheim, 1993.
(2) Wright, J. D. *Molecular Cyrstals*; Cambridge University Press: Cambridge, 1995.
(3) Law, K. Y. *Chem. Rev.* **1993**, *93*, 449−486.
(4) De Boer, S.; Wiersma, D. A. *Chem. Phys. Lett.* **1990**, *165*, 45−53.
(5) West, W.; Carroll, B. H. *The Theory of the Photographic Process*, 3rd ed.; James, T. H., Ed.; The Macmillian Co.: New York, 1966; pp 233−277.
(6) Fabian, J.; Nakazumi, H.; Matsuoka, M. *Chem. Rev.* **1992**, *92*, 1197−1226.
(7) Czikkely, V.; Försterling, H. D.; Kuhn, H. *Chem. Phys. Lett.* **1970**, *6*, 11−14.
(8) Lehn, J.-M. *Angew. Chem., Int. Ed. Engl.* **1990**, *29*, 1304−1319. Ringsdorf, H.; Schlarb, B.; Venzmer, J. *Angew. Chem., Int. Ed. Engl.* **1988**, *27*, 113−158.
(9) Ulman, A. *An Introduction to Ultrathin Organic Films from Langmuir−Blodgett to Self-Assembly*; Academic Press: New York, 1991. Roberts, G. G. *Adv. Phys.* **1985**, *34*, 475−512. Ohring, M. *The Materials Science of Thin Films*; Academic Press: New York, 1992.
(10) Daehne, L. *J. Am. Chem. Soc.* **1995**, *117*, 12855−12860. Daehne, L.; Biller, E. *Adv. Mater.* **1998**, *10*, 241−245.
(11) Daehne, L.; Biller, E.; Baumgärtel, H. *Angew. Chem., Int. Ed. Engl.* **1998**, *37*, 646−649.
(12) Daehne, L.; Tao, J.; Mao G. *Langmuir* **1998**, *14*, 565−568.

10.1021/ja983842v CCC: $18.00
Published on Web 03/24/1999

of the films and the molecular aggregation processes. But first the principles behind this research are reviewed briefly.

Spherulitic Growth in Undercooled Melt. The TLA method uses the self-organization of molecules to spherulites in highly undercooled melts,[13] which is well-known for polymers.[14] The undercooling, ΔT, is defined as $\Delta T = T_M - T$, T_M being the melting point of the crystalline film, and T being the far-field ambient temperature. Spherulitic crystallization refers to the radial growth of long thin crystals, where new crystals are generated by noncrystallographic branching continuously as the radius increases. The common condition for spherulitic crystallization is a highly viscous, undercooled liquid containing impurities or a "transient" impurities partition at the interface of a crystallizing solid. A typical spherulite was described as needles, fibers, or ribbons fanning out from the center with extensive branching. Sometimes a sheaf-like center was observed during the early stage of spherulitic crystallization. These universal morphologies were observed in very different materials: silicates in natural rocks,[15] several metals,[16] some inorganic[17] and organic materials,[18] and most polymers,[19] suggesting a mechanism independent of specific molecular structure. Although extensive investigations were conducted on this type of crystallization, the molecular origin of this process is still a controversial and somewhat mysterious topic.

One particular pattern called the banded or ringed spherulite has been the subject of many theories and discussions.[19−26] Between crossed polarizers periodic patterns of concentric rings or bands were observed in some spherulites of polymers,[20] and occasionally small organic molecules and minerals.[21] These rings arise from changes in the refractive index in the spherulite. As to the origin of this phenomenon, several mechanisms were discussed and will be briefly summarized here. (1) Secondary nucleation on growing crystals was proposed based on the similarity between the spherulitic and dendritic crystallization.[22] (2) In the helically twisting fiber model,[23] optically uniaxial crystallites were found to orient with their optical axes in the tangential direction of the spherulite. Optical, electron microscopy, and X-ray micro-diffraction experiments show that the polyethylene chain axis, always the *c* axis, spirals around the radial direction, always the *b* axis. The alternating dark and bright rings are the results of cooperative twists of the crystallites around the radial direction. (3) Other researchers have explained the periodic structure based on the diffusional segregation of impurities during crystallization leading to alternating crystalline and amorphous domains or polymorphic crystal structures.[24] (4) Oscillating changes of the temperature near the temperature of the highest growth rate due to the heat of fusion were also cited as a reason for the variation of the molecular alignment and the resulting ring formation.[25] (5) In the auto-orientation theory the banding was explained by mechanical stresses generated by the attachment of molecules with highly anisotropic shape at the interface.[26] The length of the crystallite in the direction of the attached polymer chain was assumed to increase several hundred percent upon crystallization. Hence, the surrounding molecules in the amorphous phase reorient perpendicular to those in the crystalline phase to compensate for the dimensional changes. Experimental bases of the above theories have been lacking primarily due to the difficulty in identifying the exact molecular orientation and supramolecular architecture in the banded spherulite, which invariably possesses a high degree of structural inhomogeneity. With the current system of the BDH^+ dye where not only the optical axes are clearly defined but also the crystal structure and the crystal orientation are measurable, it is hopeful that the molecular origin of the banded structure together with the curved growth can be finally resolved experimentally.

Structure and Properties of J-Aggregates. Due to the strong van der Waals dispersion forces, polymethine dyes readily form aggregates in solutions, on surfaces, and in solids. Based on indirect evidence, the internal structure of J-aggregates[27] is widely perceived as arrays of tightly packed molecules with their molecular planes stacked parallel against each other.[28] Interactions between molecular transition dipoles lead to the formation of excitons and to a shift of absorption energy to blue (H-aggregates) or to red (J-aggregates) with respect to the monomer absorption, as well as to an increase in the absorption coefficient due to a narrowing of the absorption band.[29] When there are two different molecular orientations in the unit cell, the molecular transition splits into two excitonic components m_+ and m_- which are perpendicular to each other.[29] In Figure 1, the J-aggregates of two stacking directions A_1 [110] and A_2 [1$\bar{1}$0] in $BDH^+ClO_4^-$ single crystals are defined by the following parameters: the dislocation angle α, the intermolecular distance d, and the angle τ between two molecular directions resulting in two excitonic components m_+ and m_-.

Due to their high absorption coefficient, 3-D arrays of J-aggregates become strongly polarized by light. The interaction of the anisotropic polarization with the excitons is described by polaritons.[30] The main effect of polaritons is a directional dispersion of the absorption energy. Depending on the angle β between the transition dipole moment and the incoming light, the absorption energy of the solid shifts from the transverse exciton energy at $\beta = 90°$ to the higher longitudinal exciton energy at $\beta = 0°$. In strongly absorbing solid materials such as BDH^+ crystals, the difference between transverse and longitudinal energy can reach more than 10 000 cm^{-1}.[31] In case of the investigated $BDH^+ClO_4^-$ salt two excitonic absorption

(13) Khoury, F.; Passaglia, E. In *Treatise on Solid State Chemistry, Vol. 3, Crystalline and Noncrystalline Solids;* Hannay, N. B., Ed.; Plenum: New York, 1976; Chapter 6.

(14) Sperling, L. H. *Introduction to Physical Polymer Science, 2nd ed.*; John Wiley and Sons: New York, 1992; pp 218−244.

(15) Johannsen, A. *Descriptive Petrography of Igneous Rocks*; University of Chicago Press: Chicago, 1931.

(16) *The Solidification of Metals* (Proceedings of the Brighton, England Conference), The Iron and Steel Institute: London, 1968; pp 256−264.

(17) Morse, H. W.; Donnay, J. D. H. *Am. Mineral.* **1933**, *18*, 66−67.

(18) Bernauer, Gedrilte Kristalle, Borntrager, Berlin, 1929.

(19) Keller, A. *Nature* **1952**, *169*, 913−914. Keith, H. D.; Padden, F. J., Jr. *J. Appl. Phys.* **1963**, *34*, 2409−2421.

(20) Keith, A. *J. Polym. Sci.* **1955**, *17*, 291−308. Keith, H. D.; Padden, F. J. *J. Polym. Sci.* **1959**, *39*, 101−122. Price, F. P. *J. Polym. Sci.* **1959**, *39*, 139−150.

(21) Wallerant, F. *Bull. Soc. Franc. Mineral.* **1907**, *30*, 45−60.

(22) Tiller, W. A. *The Science of Crystallization: Macroscopic Phenomena and Defect Generation;* Cambridge University Press: Cambridge, 1992; pp 322−324, 342−347.

(23) Keith, H. D.; Padden, F. J. *J. Appl. Phys.* **1959**, *30*, 1479−1484. Bassett, D. C. *Principles of Polymer Morphology;* Cambridge University Press: Cambridge, 1981; pp 19−22. Young, R. J.; Lovell, P. A. *Introduction to Polymers*, 2nd ed.; Chapman & Hall: London, 1991; pp 261−264.

(24) Keith, H. D.; Padden, F. J. *J. Polym. Sci.* **1961**, *51*, S4−S7.

(25) Foks, J. *Polym. Commun.* **1990**, *31*, 255−258.

(26) Schuur, G. *J. Polym. Sci.* **1961**, *L*, 191−209. Burns, J. R. *J. Polym. Sci.* **1969**, *7*, 593−600. Calvert, P. D.; Uhlmann, D. R. *J. Polym. Sci.* **1979**, *11*, 457−465.

(27) Scheibe, G. *Angew. Chem.* **1937**, *50*, 212−219. Jelly, E. E. *Nature* **1937**, *139*, 631−632. Hurtz, A. H. *Adv. Colloid Interface Sci.* **1977**, *8*, 237−298. Harrison, W. J.; Mateer, D. L.; Tiddy, G. J. T. *J. Phys. Chem.* **1996**, *100*, 2310−2321.

(28) Davydov, A. S. *Theory of Molecular Excitons;* Plenum Press: New York, 1971.

(29) Kasha, M.; McRae, E. G. *Physical Processes in Radiation Chemistry;* Augenstein, L., Ed.; Academic Press: New York, 1964; pp 23−42.

(30) Mills, D. L.; Burstein, E. *Rep. Prog. Phys.* **1974**, *37*, 817−925. Small, G. J.; Connolly, M. A.; Stevenson, S. H. *Chem. Phys.* **1988**, *128*, 157−168.

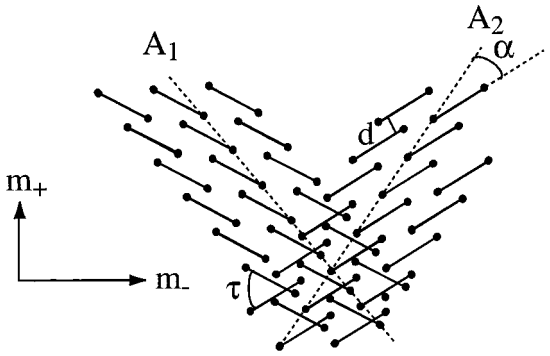

Figure 1. J-aggregate structure in $BDH^+ClO_4^-$ single-crystal according to X-ray diffraction: intermolecular distance $d = 3.54$ Å, stacking or dislocation angle $\beta = 29.7°$, angle between the two molecular directions $\tau = 68.5°$. A_1 and A_2 are the aggregate directions, m_+ and m_- are the bisectors of the two molecular directions and therefore the excitonic absorption components. The circles correspond to the nitrogen atoms of the BDH^+. The rods represent the polymethine chain.

components were observed in the single crystal by reflection spectroscopy.[32] The m_+ component parallels the [201] crystal axis and absorbs light at 639 nm, when oriented perpendicular to the incident light beam. Due to the polariton effect the absorption wavelength decreases with decreasing β until the longitudinal energy of 430 nm. The m_- component is oriented along the [010] axis and absorbs light between 589 nm for $\beta = 90°$ and at 353 nm for $\beta = 0°$. [010] and [201] are perpendicular to each other.

The red-shifted J-aggregate band is also influenced by the shape and the effective size or the amount of coherently coupled molecules of the J-aggregate. This value was estimated to be in the range of 4 to 20 molecules by photon echo experiments, while the physical size of the J-aggregate can be much larger.[33] The recently developed scanning probe microscopy (SPM) techniques such as scanning tunneling microscopy (STM), atomic force microscopy (AFM), and near field scanning optical microscopy (NSOM) push the lateral resolution to the angstrom level promising to finally resolve the molecular structure of J-aggregates.[34] STM offers the highest resolution, but it also requires an electrically conductive film. STM has been used to image thin insulating layers up to a few monolayers,[35] but the question remains whether an insulating layer of 80 nm in thickness can be imaged by STM. NSOM was used to probe elegantly the absorption and fluorescence properties of J-aggregates in the nanometer scale,[36] but the method has not yet reached the spatial resolution of AFM and STM. We attempted to image the microstructure of J-aggregates in a thin solid film state using both AFM and STM.

Experimental Section

Materials. The chemical structure of the dye perchlorate salt $BDH^+ClO_4^-$ is shown in Scheme 1. The $BDH^+ClO_4^-$ was obtained by exchanging Cl^- with ClO_4^- in BDH^+Cl^-, which was synthesized according to the literature.[37] The dye compounds were kept away from light and water to avoid photolytic and hydrolytic degradation. Large single crystals (5 mm in length) with green golden color and perfect habit were grown from dry acetone. The purity of the dye crystals was confirmed by spectroscopic methods such as UV/vis, NMR, and mass (FAB+) spectroscopy. The maximum absorption occurred at 510 nm with an extinction coefficient of 190 000 L mol^{-1} cm^{-1}. The melting point of the crystal was measured to be 177−179 °C. HPLC grade acetone with purity >99.7% was purchased from Fisher Scientific and used as received. Quartz glass substrates of 10 × 10 mm^2 (G. M. Associates) were cleaned with acetone and rigorously dried before use.

Scheme 1. Chemical Structure of Dye Salt 1,7-Bis(dimethylamino)heptamethine Perchlorate ($BDH^+ClO_4^-$).

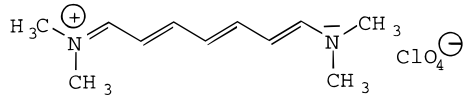

Film Preparation by Thin Layer Aggregation (TLA). The ordered dye films were prepared in two steps.[10] First, 1×10^{-2} to 3×10^{-2} mol/dm^3 solutions of $BDH^+ClO_4^-$ in acetone were placed on quartz, and amorphous dye films were obtained by spin coating at room temperature with a spin rate of 3000 rpm (PM101DT-R485 Photo Resist Spinner, Headway Research Inc.). Depending on the solution concentration, amorphous films of thickness between 30 and 150 nm were obtained. For most investigations films of approximately 80 nm thickness were used. The thickness was determined by complete dissolution of the dye film in methanol and subsequent spectroscopic determination of the dye amount. The density of the layer was assumed to be 1.263 g/cm^3, the same as the single crystal. Spectroscopic investigation of the layer transmission within the amorphous film reveals a thickness variation in an area of 100 mm^2 to be below 2%. In the second step the amorphous phase was transformed into crystalline spherulites. Nuclei formed spontaneously, which expanded spherically up to 1 cm in diameter. The temperature dependence of the nucleation and the growth process was investigated at constant absolute air humidity of 11.5 g/m^3 in an oven with a temperature set in the range between 20 and 150 °C. A microscope (Olympus) with a homemade, electronically controlled heating stage was used for the kinetic study of the TLA process. The kinetics of the growth process was followed by a video microscope with a temporal resolution of 20 ms. At high temperatures the film could be significantly colder than the heating stage due to high growth rate and slow thermal conduction through the substrate. The real temperature of the growth process was estimated by taking the thermal conduction into account. The rate of the thermal conduction was determined by measuring the time needed for the melting of reference substances on the hot stage.

Crystal Structure. The structure of $BDH^+ClO_4^-$ single crystals was determined by X-ray diffraction.[38] The crystal structure belongs to the monoclinic space group $C2/c$ with lattice parameters $a = 11.60$ Å, $b = 8.803$ Å, $c = 15.25$ Å, and $\beta = 109.7°$. The main structural feature is the plane-parallel arrangement of dye molecules in 1-D staircase aggregates as shown in Figure 1. These aggregates are arranged parallel to each other in the (001) layers, but every second layer is rotated with respect to the other one, yielding two molecular and aggregate directions, A_1 [110] and A_2 [1$\bar{1}$0]. The layers are separated from each other by the ClO_4^- anions.

Optical Spectroscopy. The optical spectra of the films were recorded in transmission with a Universal Microscope Spectral Photometer UMSP 80 (Carl Zeiss, Oberkochen) with quartz optics. The light source was a 75 W xenon lamp dispersed by a grating monochromator and polarized by a calcite polarizer. The polarizer was positioned between the light source and the sample to reduce the decomposition of the dye by the focused light beam to less than 2% per measurement. The transition direction was measured by automated rotation of the polarizer at the wavelength of the absorption maximum. The angle for the lowest

(31) Daehne, L.; Kamiya, K.; Tanaka, J. *Bull. Chem. Jpn.* **1992**, *65*, 2328−2332.
(32) Daehne, L.; Horvath, A.; Weiser, G. *Chem. Phys.* **1995**, *196*, 307−316.
(33) Spano, F. C.; Mukamel, S. *J. Chem. Phys.* **1989**, *91*, 683−699. De Boer, S.; Wiersma, D. A. *Chem. Phys. Lett.* **1990**, *165*, 45−53.
(34) Binnig, G.; Quate, C. F.; Gerber, Ch. *Phys. Rev. Lett.* **1986**, *12*, 930−933. Betzig, E.; Trautman, J. K.; Harris, T. D.; Weiner, J. S.; Kostelak, R. L. *Science* **1991**, *251*, 1468−1470.
(35) Sarid, D. *Scanning Force Microscopy: with Applications to Electric, Magnetic, and Atomic Forces;* Oxford: New York, 1991. DeRose, J. A.; Leblanc, R. M. *Surf. Sci. Rep.* **1995**, *22*, 73−126.
(36) Higgins, D.; Barbara, P. F. *J. Phys. Chem.* **1995**, *99*, 3−7. Higgins, D. A.; Reid, P. J.; Barbara, P. F. *J. Phys. Chem.* **1996**, *100*, 1174−1180. Higgins, D. A.; Kerimo, J.; Vanden Bout, D. A.; Barbara, P. F. *J. Am. Chem. Soc.* **1996**, *118*, 4049−4058.
(37) Nikolajewski, E.; Daehne, S. *Chem. Ber.* **1967**, *100*, 2616−2619.
(38) Daehne, L.; Reck, G. *Z. Kristallogr.* **1995**, *210*, 40−43.

transmittance was set as the transition direction. The spectra were obtained from a measuring field of $10 \times 10\ \mu m^2$.

Atomic Force Microscopy (AFM) and Scanning Tunneling Microscopy (STM). A nanoscope IIIa (Digital Instruments) was used to investigate the surface morphology of $BDH^+ClO_4^-$ films. Quartz substrates with spin coated dye thin films were glued onto stainless steel disks, and scanned with the Contact Mode in ambient air at room temperature. A 109 μm j scanner or a 16 μm e scanner was used, calibrated by a standard 1 μm unit length gold calibration ruling and/or mica substrates. Silicon nitride tips with a spring constant of 0.06 N/m and a nominal tip radius of curvature of 20 to 40 nm were used. Different scan angles were used to trace and retrace the same surface area to detect any tip-induced artifacts. All images were captured in the height mode where the force between the tip and surface was kept constant. To prevent the decomposition of the layer by the laser light and to obtain a higher spatial resolution, a 12 μm STM scanner with Pt−Ir STM tips was also used to profile the surface. The quartz substrate was coated with palladium.

In the real time measurement of growth processes, the growth rate of the spherulites was adjusted by the air humidity. The spherulitic growth rate can be changed from 0.2 to 3 $\mu m\ s^{-1}$ by increasing the air humidity from 30 to 60%. The real time measurements were performed in a sealed box, where the growth rate of the spherulite was adjusted by using various saturated salt solutions. Photochemical decomposition of the $BDH^+ClO_4^-$ film not yet crystallized was observed with repeated scans, induced by the laser. The laser-generated products reduced the growth rate and increased the roughness of the crystallized region. To minimize the laser-induced degradation, the laser was switched on only after the completion of the rest of AFM setup, and scanning immediately followed.

Results

Approximately 80 nm thick amorphous films of the $BDH^+ClO_4^-$ salt were aggregated at temperatures between 20 and 150 °C. Although other factors mentioned above also influence the spherulitic growth processes, this paper focuses on the temperature effect. Spherulitic growth between 90 and 150 °C (low undercooling) yielded simultaneously two types of macroscopic domains of homogeneous supramolecular architecture (Figure 2a). The light absorption is strongly anisotropic (dichroic) as observed in linearly polarized light. For light polarized in the radial direction of the spherulite both domains are colorless and highly reflective, but for light polarized in the tangential direction, one region exhibits a blue color (blue/colorless region BC), and the other region a red one (red/colorless region RC).

TLA at temperatures below 90 °C (high undercooling) resulted in a film with intermittent changes of color (banding) of the RC domain in the radial direction (Figure 2b). For light polarized along the radial direction, the film color changes within one band from colorless, yellow, red, purple, to blue, and starts again with colorless. For the light polarized in the tangential direction the color of the band is uniformly red. The various color regions melt simultaneously at 155−157 °C, pointing to the same crystal structure. In addition, the optical spectra of the dye film are quite similar to those of the single crystal, displayed in Figure 3, which also suggests the same crystal structure. The detailed analysis of the spectra was presented elsewhere and will not be repeated here.[12] The important feature is the close match between the spectra from the RC film and the single crystal (201) face and that from the BC film and the (010) face. Both spectra are red-shifted from the monomeric ones centered at 510 nm. The results will be presented in three sections, which consist of the kinetics of the growth process, the growth at low undercooling, and the growth at high undercooling.

J-Aggregation and the Spherulitic Growth Process. After removing the solvent by spin coating, an amorphous film of $BDH^+ClO_4^-$ was obtained, as shown by the complete light quenching between crossed polarizers. The absorption maximum of the amorphous layer overlaps that of a dilute solution of $BDH^+ClO_4^-$ (Figure 3). The absorption band is broadened significantly due to the random transition dipole interactions in the film.

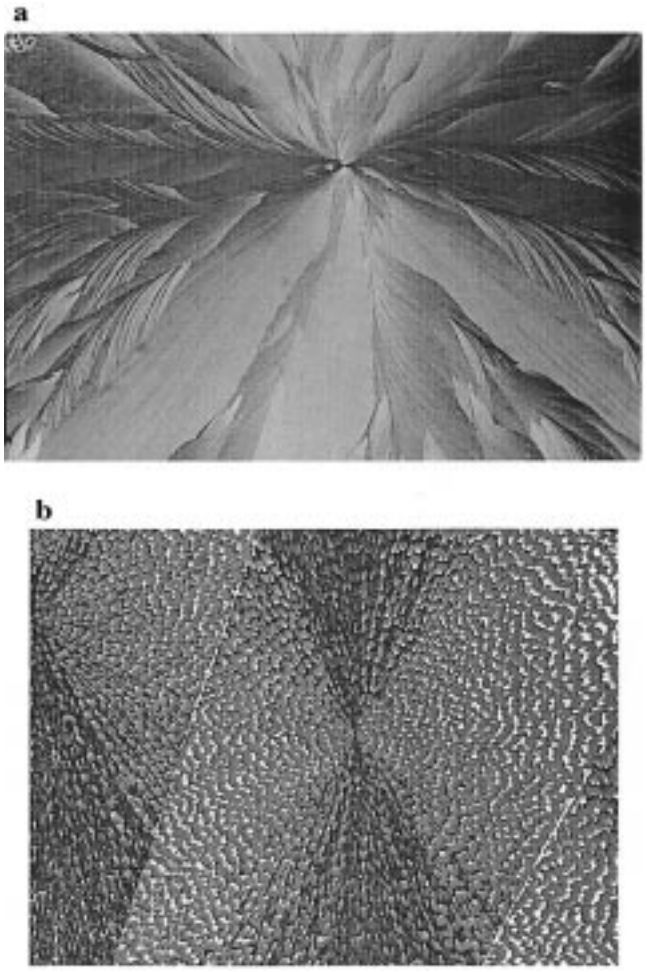

Figure 2. Microphotographs of $BDH^+ClO_4^-$ spherulites. (a) A spherulite of coexisting RC and BC regions crystallized at a low undercooling temperature of 110 °C. The size of the picture is 0.9 mm × 0.6 mm. The polarization direction is vertical. (b) Banded spherulites crystallized at a high undercooling temperature of 88 °C. The size of the picture is 2.3 mm × 1.7 mm. The polarization direction is horizontal. The photos were taken in transmission with linearly polarized light. Unlike similar pictures in the literature only one polarizer was used here. One polarizer allows the observation of the real dichroic colors and excludes color effects induced by interference or birefringence.

After some minutes of induction time, nuclei formed spontaneously in the amorphous phase. Their growth rate depends strongly on temperature as shown in Figure 4. The growth rate was almost constant at 0.35 $\mu m\ s^{-1}$ at temperatures below 40 °C, rose to 550 $\mu m\ s^{-1}$ at 135 °C, and decreased rapidly above 135 °C. The radial growth rate was constant at a constant temperature, suggesting an interface controlled process, where the rate determining step is the molecular attachment at the interface rather than the molecular diffusion to the interface. However, it should be pointed out that at high undercooling where the banded structure develops, our data indicate a fluctuation in the radial growth rate. These periodic fluctuations cannot be measured due to the limited spatial resolution of the video camera. But the wavy grain boundary between two banded spherulites, captured by AFM (see Figure 9d), indicated a gradually decreasing growth rate within a band.

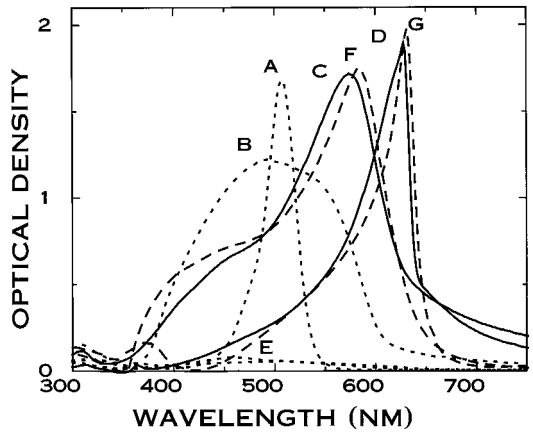

Figure 3. Optical spectra of $BDH^+ClO_4^-$ in solution with maximum optical density at 510 nm (A), spin-coated films of the amorphous phase with a broad band maximum at 510 nm (B), RC film polarized along the tangential direction with a maximum at 574 nm (C), BC film polarized along the tangential direction with a maximum at 628 nm (D), RC and BC polarized along the radial direction (E), the m_- exciton component [010] in the (201) plane of the single crystal with a maximum at 591 nm (F), and the m_+ component [201] in the (010) plane of the single crystal with a maximum at 639 nm (G).

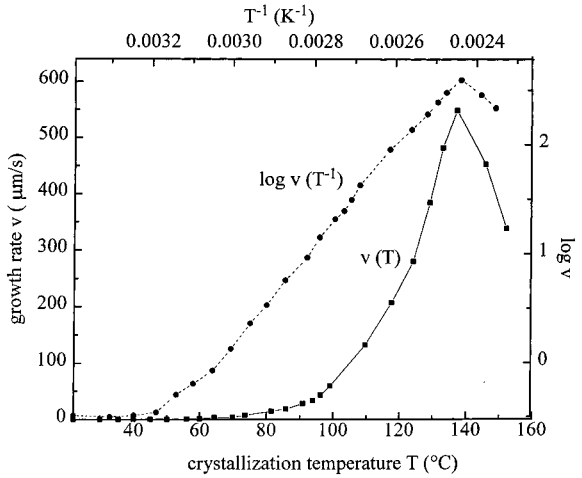

Figure 4. Spherulite radial growth rate, *V*, as a function of crystallization temperature, *T*. The plot of *V* versus *T* is represented by squares and the interpolated continuous line, while the log *V* versus 1/*T* plot, which was used to determine the activation energy Q_A for the molecular attachment at the interface, is represented by the circles and the interpolated dashed line.

The moving interface between the crystalline and amorphous phase was investigated by AFM in real time at room temperature and 12 g/m^3 air humidity. As expected, the surface of the amorphous phase is featureless and molecularly smooth with a mean roughness Ra = 1.2 nm, which is 1.5% of the total film thickness. The surface became grainy after crystallization where Ra rose to 8.7 nm (Figure 5a). The height profile (Figure 5b) shows an increase in the local layer thickness right after crystallization, which is coupled by a deep depression in the amorphous phase. In contrast, a smaller local layer thickness in the crystalline phase at another spot is coupled with a shallower depression in the amorphous phase. The real time image captured the flow of molecules in the highly viscous amorphous phase in order to attach and orient at the crystalline front.

RC and BC Films Prepared at Low Undercooling. The two dichroic regions RC and BC were prepared by aggregation of the amorphous phase at temperatures between 90 and 130

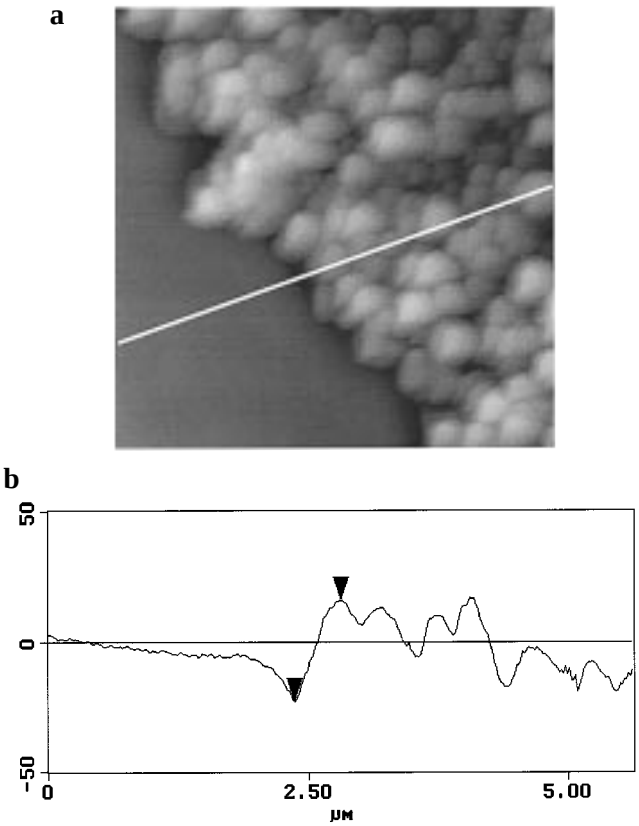

Figure 5. (a) Real time AFM measurement of the crystalline and amorphous phase boundary in the $BDH^+ClO_4^-$ spherulite at 25 °C. Scan size = 5 μm, and *z* range = 100 nm. (b) The height profile of the crystallizing front along the white line in part (a), showing the flow of molecules from the amorphous phase to the crystal phase. The vertical peak-to-valley distance between the two arrows is 39 nm.

°C. Sometimes the two regions coexist (Figure 2a), but other times, the spherulite primarily consisted of one region. The ratio between the two regions cannot be precisely controlled, suggesting an almost identical radial growth rate for the two regions. The RC region of the spherulite always exhibits a straight radial growth, but the BC region tends to grow into curves, bent to the right or left of the radial direction *R*.

AFM and STM images of the RC region are displayed in Figure 6a−c. The topography is made of ray-like fibers straight from the center to the periphery of a spherulite as shown in Figure 6a with a mean surface roughness Ra = 8.4 nm. At the micron level as shown in Figure 6b, no crystalline features such as ledges or terraces were found. The lack of large crystalline faces at the film surface has prevented the molecular resolution by AFM and direct probing of the BDH^+ orientation within the layer. STM is capable of a better lateral resolution due to its much sharper tip and tunneling mechanism. Therefore, the RC film was also investigated by high-resolution STM and is displayed in Figure 6c with the same scan size of 1 μm as in Figure 6b. The aggregates averaging 0.1 μm in diameter in Figure 6b were made up of even smaller grains in the 10−20 nm size range. These particles were different in size and distributions from the palladium surface also imaged by STM. It is intriguing that the uniform orientation of J-aggregates is not reflected in the surface topography at the nanometer scale, while it is clearly demonstrated by optical studies of the same film. However, this lack of macroscopic crystalline features is often observed in materials consisting of J-aggregates, which was attributed often to packing faults or impurities.[36] The small size of ordered domains also is expected of the spherulitic

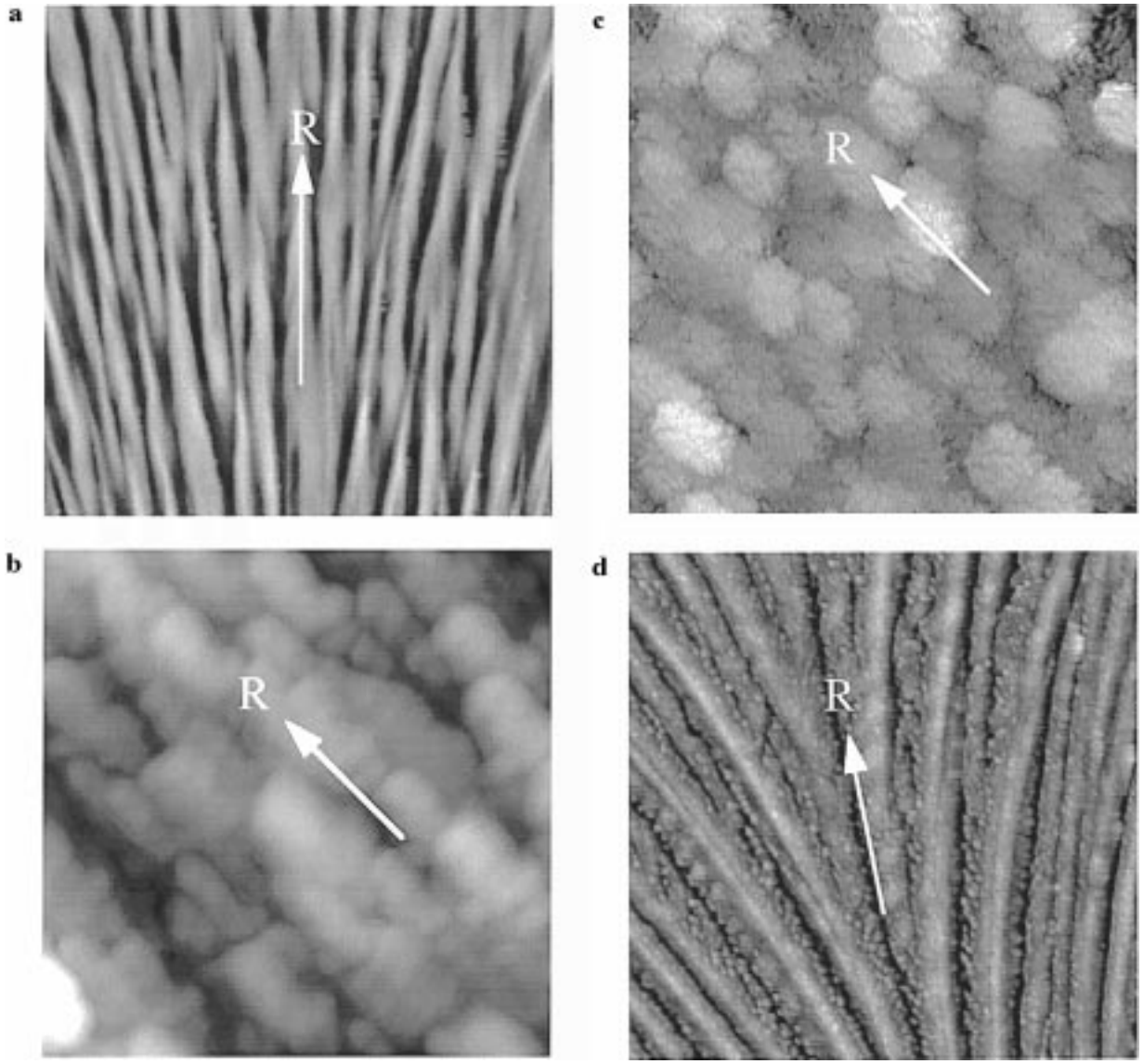

Figure 6. AFM and STM images of the RC and BC regions crystallized at 110 °C. *R* is the radial direction. (a) AFM of the RC region consisting of straight fibers along the radial *R* direction. Scan size =30 μm, and *z* range = 200 nm. (b) AFM of the RC region. Scan size = 1 μm, and *z* range = 40 nm. (c) STM scan of the RC region. Scan size = 1 μm, and *z* range = 30 nm. (d) AFM of the BC region consisting of right- and left-handed curves. Scan size = 30 μm, and *z* range = 200 nm.

crystallization, where the local roughness is expected to reach the dimension of the size of the mosaic blocks of the substructure in the crystalline fibers.[39] In addition, large crystalline domains on the surfaces of the RC and BC films are not possible, since neither the (201) nor the (010) face is a low-energy crystal face, concluded from their absence in single crystals. The Rodlike BDH^+ molecules as well as the aggregates protruding out of the (201) and (010) face resulted in a nonplanar surface. It is surprising that the electrical conductivity of the dye layer was high enough for STM measurements despite its 80 nm thickness. This result is consistent with an increase of the DC conductivity by 5 orders in BDH^+ crystals containing J-aggregates in respect to those where no aggregate stacks exist.

In contrast to the RC region the topographical pattern of the BC region varies greatly depending on the air humidity, temperature, layer thickness, and the time between spin coating and heating. Besides the coexisting V-shaped or herringbone fibers,[12] domains of right-handed only or left-handed only curves were obtained with a high roughness of Ra = 23 nm (Figure 6d). The spherulitic patterns are better defined in the BC region with deep valleys between fibers of aggregates. The physical size of the aggregate is also larger.

The difference in surface morphology of the BC and RC regions was also revealed by AFM in under-deposited $BDH^+ClO_4^-$ films. Figure 7a shows the BC and RC regions of a film spin coated at a lower dye concentration which effectively reduced the film thickness. The height profile of the image is shown in Figure 7b. The exposed substrate surface between the dye fibers provided the reference for film thickness estimation. The film thickness of the RC phase was 40 nm and that of the BC phase 72 nm. The increase of thickness in the BC domain causes the formation of deep valleys between the fibers by shrinkage and dewetting. This points to a higher growth rate in the fiber thickness direction [010], which is normal to the film surface, than in [201], which is the tangential direction of the spherulite.

Banded Spherulites Formed at High Undercooling. At a temperature range between 20 and 90 °C, banded spherulites were formed (Figure 2b) with the intermittent changes of color. The length of the banding periodicity was investigated by spatial

(39) James, R. W. *The Optical Principles of the Diffraction of X-Rays;* G. Bell: London, 1948.

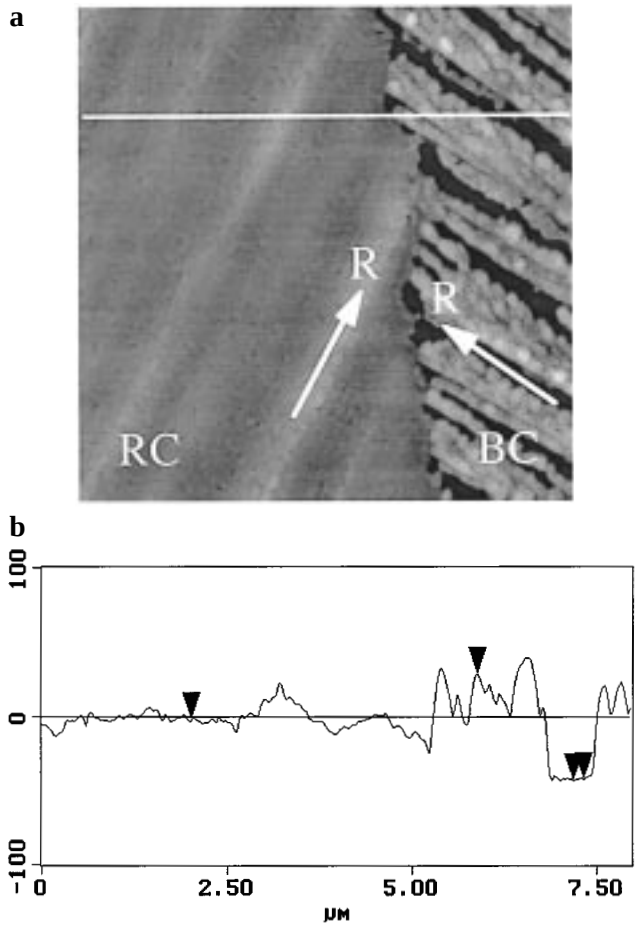

Figure 7. AFM of under-deposited $BDH^+ClO_4^-$ spherulite consisting of a continuous RC region and a discontinuous BC region. (a) AFM top view image of the RC and BC boundary. Scan size = 4 μm, and z range = 200 nm. (b) The height profile along the white line in part (a), showing a film thickness of the RC region (40 nm) and of the BC region (72 nm).

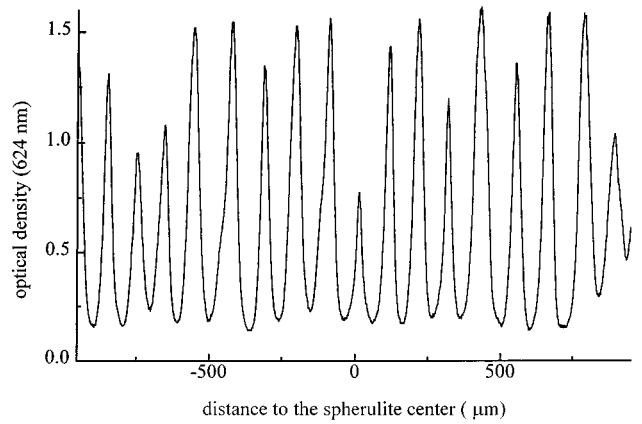

Figure 8. Line scan of the optical density at 624 nm along the radial direction of a $BDH^+ClO_4^-$ spherulite crystallized at 88 °C. The light is polarized along the radial direction.

scans of the optical density in the radial direction of the spherulites with use of a linearly polarized light with a wavelength of 624 nm (Figure 8). The peaks correspond to the blue region of a color band, whereas the other regions show almost no absorption at this wavelength. The periodicity of the colored bands is highly regular. Neither the peak height nor the period length changes significantly during the growth. The length of the period diminishes with decreasing temperature from 100 μm at 88 °C to 2 μm at 40 °C, as well as with decreasing layer thickness. Below 40 °C, the period was too small to be resolved by optical microscopy, but large enough to be imaged by AFM (Figure 9a). At 25 °C the period was irregular and the surface was covered by grainy features with Ra = 4.5 nm. With increasing temperature, the oscillating period increases, and fanlike features with their tails pointing outward and tips pointing toward the center of the spherulite became more distinctive. Figure 9b shows an AFM image of a layer formed at 70 °C with Ra = 8.9 nm. The height profile along the radial direction is displayed in Figure 9c. The average length of the fan from the tip to the next one along the radial direction was estimated to be about 20 μm. The average height difference between the highest point in the tip section and the lowest point in the tail section of a fan is about 35 nm. By comparing the optical and topographical features of the banded spherulite, it became apparent that the tip of the fan with the highest film thickness is the red/colorless RC region, and that the tail of the fan with the lowest film thickness is the red/blue region.

While the direction of the m_- component remains unchanged in the tangential direction, which yields the constant red color, the m_+ component rotates around the tangential axis from the upright direction at the colorless tip to the radial, planar direction at the blue tail (Figure 9c). With increasing periodic length the height difference between the tip and the tail diminishes. The wavy boundary shown in Figure 9d indicates a fluctuation in growth rate of various color regions within one band. In the case of the uniform growth rate, the spherulitic boundary is straight as exhibited by the RC film. But for the banded spherulite as shown in Figure 9d of an enlarged section of the boundary, a convex shape was formed at point *A* by the tip portion, approximately 4.5 μm out of the total fan length of 20 μm, from the right spherulite impinging upon the tail portion from the left spherulite. This implies a higher growth rate of the colorless region than that of the blue region.

Discussion

Kinetics of the Spherulitic Growth Process. Our study of $BDH^+ClO_4^-$ spherulitic growth kinetics agrees in general with previous experimental study on polymers and melt crystallization of other materials: (1) the radial growth rate was linear in time, and (2) the growth rate goes through a maximum as the temperature of crystallization is lowered.[14] The temperature dependence of the growth rate of the $BDH^+ClO_4^-$ spherulites shown in Figure 4 is typical of the kinetics of melt crystallization.[40] At low undercooling or near equilibrium conditions, the growth rate is controlled by the rate of nucleation, which decreases with increasing temperature. This is described by the Wilson and Frenkel model for low undercooling:[41]

$$V = K\Delta\mathrm{Gn}(T_\mathrm{M} - T)$$

where V is the growth rate at temperature T, K is a proportional factor, T_M is the melting point, which is 155−157 °C for the $BDH^+ClO_4^-$ layer, and ΔGn is the enthalpy difference between the amorphous and crystalline phase. The factor $K\Delta$Gn was determined to be 10 μm s^{-1} K^{-1} from the linear part of the function V versus T between 135 and 150 °C. In this temperature range the melt growth is enthalpy driven and is not limited by the rate of molecular attachment to the interface due to the low viscosity of the amorphous phase.

(40) Wilke, K. Th.; Bohm, J. *Kristallzeuchtung;* Harri Deutsch Verlag: Frankfurt, 1988; pp 165−187. Palys, L. H.; Phillips, P. J. *J. Polym. Sci., Polym. Phys. Ed.* **1980**, *18*, 829−852.

(41) Frankel, J. *Phys. Z. Sowjetunion* **1932**, *1*, 498−536.

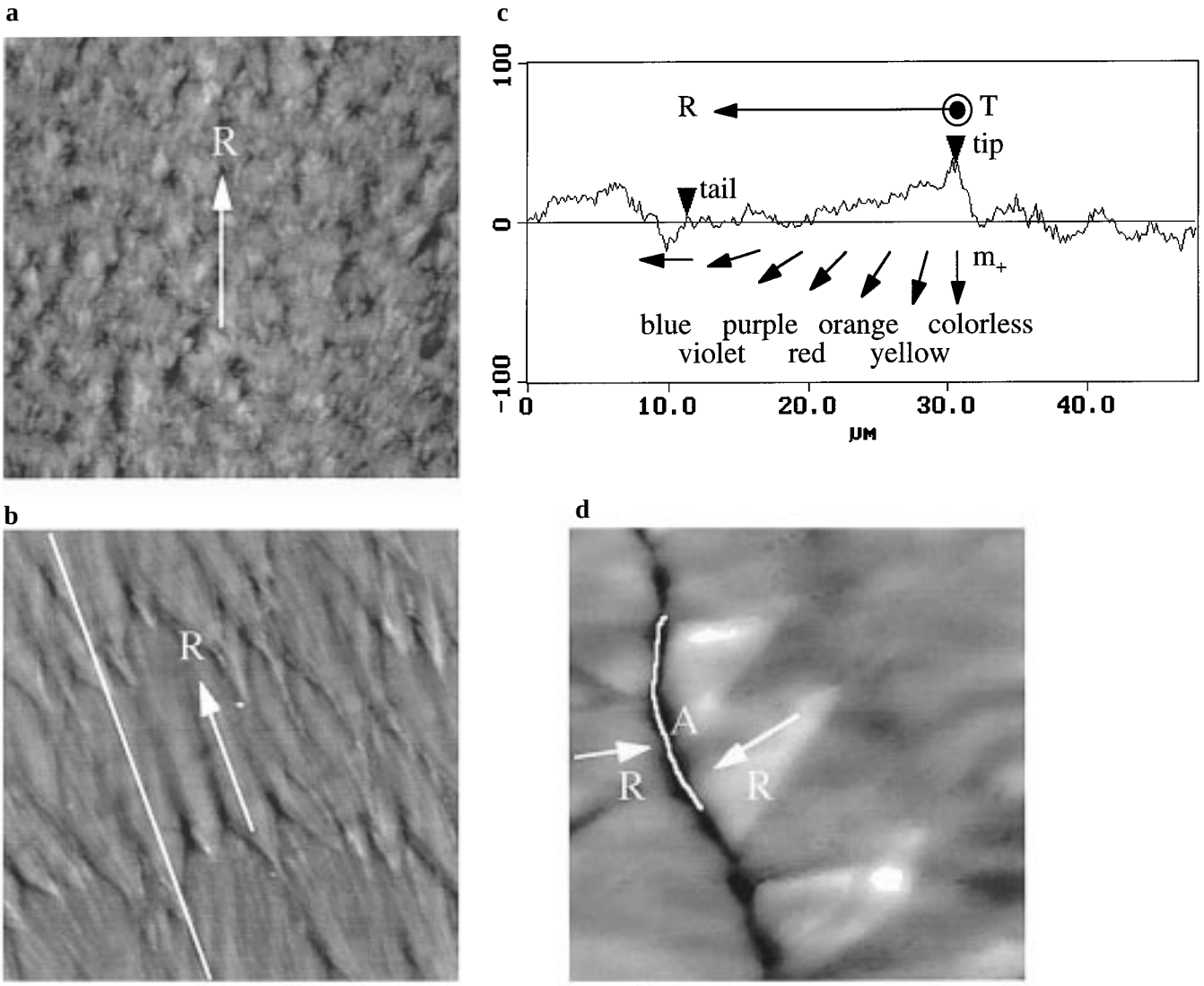

Figure 9. AFM images of the banded spherulites. (a) AFM scan of a banded spherulite crystallized at 25 °C. Scan size = 10 μm, and z range = 200 nm. (b) AFM scan of a banded spherulite crystallized at 70 °C. Scan size = 40 μm, and z range = 200 nm. (c) The height profile along the white line in part (b). The peak-to-valley distance between the tip and the tail section as indicated by the two arrows at 35 nm. The color variation and the rotation of the m_+ component around the tangential T direction were shown. For simplicity, the m_- component, unchanged along the tangential direction, is omitted here. (d) AFM scan of a convex boundary at point A, where the tip region of the right spherulite impinges on the tail region of the left spherulite. Scan size = 14 μm, and z range = 200 nm.

As the crystallization temperature is lowered, the rate of molecular diffusion competes with the rate of nucleation until reaching the maximum. At higher undercooling, the liquid-phase viscosity increases, and the growth rate now limited by the molecular diffusion and attachment to the growing crystalline front decreases. The activation energy Q_A for the molecular attachment is calculated by using the equation of Wilson and Frenkel for the kinetics in strongly undercooled melts:[42]

$$V = A \exp(-Q_A/RT)$$

From the linear part of the log V versus $1/T$ where T is between 40 and 135 °C an activation energy Q_A of 80 kJ/mol was determined for phase transition in $BDH^+ClO_4^-$ thin films. The linearity of the plot between 40 and 135 °C indicates a growth mechanism controlled by the molecular attachment to the interface. However, in the attachment limited regime, two types of growth processes were observed. At a crystallization temperature between 90 and 135 °C, a self-consistent growth process occurred producing the RC and BC region. But below 90 °C, an intermittent growth mechanism takes place, resulting in a periodic variation in the radial growth rate. Figure 9d shows the convex boundary formed by the tip of a fanlike feature impinging upon the tail of another when two banded spherulites meet. This indicates a higher growth rate of the tip. The film thickness variation within a period from the highest point at the tip to the lowest point at the tail also implies a fluctuation in temperature, viscosity, and rate of molecular diffusion during growth. Despite these changes on the molecular level, the kinetic study of both processes at low and high undercooling, conducted by the optical microscopy, agrees very well with the kinetic model of Wilson and Frenkel.

In-Plane Rotation of Molecular Axis in the BC Region. The molecular arrangement in the RC and BC region is drawn in Figure 10. This drawing is based on the X-ray diffraction data of $BDH^+ClO_4^-$ single crystal and optical match between single-crystal faces and films (Figure 3). The orientations of the m_+ and m_- components in the $BDH^+ClO_4^-$ thin film were derived based on the spectroscopic data. The RC region

(42) Turnbull, D.; Fisher, J. C. *J. Chem. Phys.* **1949**, *17*, 71−73.

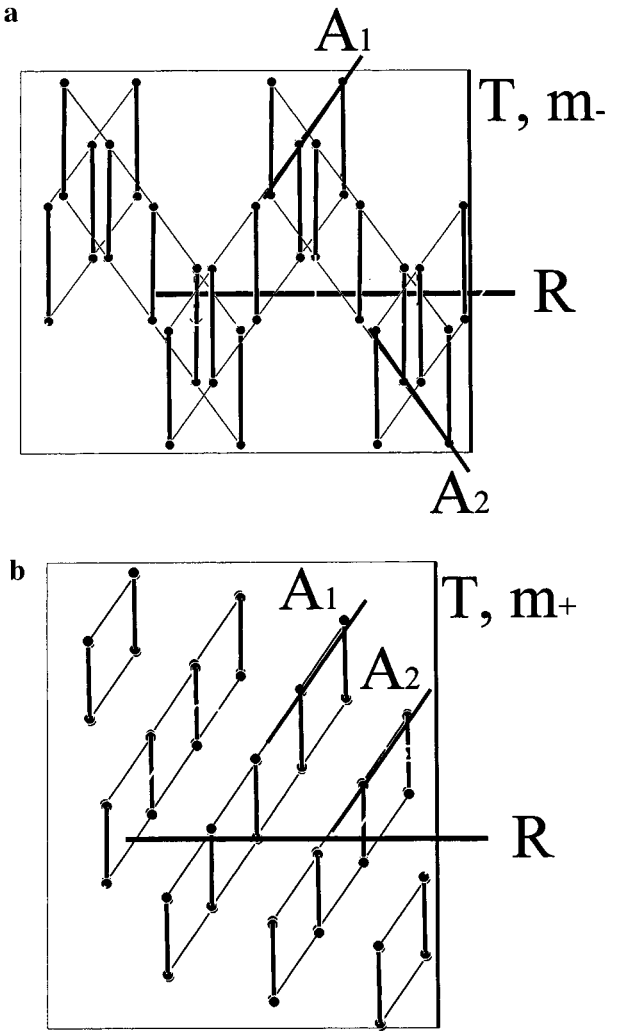

Figure 10. Models of the molecular orientation and supramolecular architecture in $BDH^+ClO_4^-$ spherulitic films crystallized at low undercooling, viewed along (a) [201] or m_+ and (b) [010] or m_-. *R* is the radial growth direction of the spherulite. *T* is the tangential direction that parallels m_- in the RC region and m_+ in the BC region. A_1 and A_2 are the two aggregate directions. The crystal structure was based on the X-ray analysis of single crystals.

corresponds to the (201) face of the single crystal as depicted in Figure 10a. The m_- component is in the tangential direction *T* or [010] axis, which gives the red color. The m_+ component is perpendicular to both *T* and the radial direction *R* or [10$\bar{2}$] axis, hence, a normal incident light cannot be absorbed by this component. The BC region represents the (010) face where the m_+ component is along *T*, giving the blue color, and the m_- component is perpendicular to the film surface, as shown in Figure 10b. Region BC has the same crystal structure and growth direction as RC, but the crystal lattice is rotated by 90° around the [10$\bar{2}$] axis.

Notice the molecules in both regions are always in a plane that is perpendicular to *R*, in other words, the molecules always attach parallel to the spherical growing front. In spherulitic growth of polymers, the individual chains were also believed to fold back and forth tangentially to the growing spherical surface of the spherulite.[14] Due to the strong attraction between the molecules attaching parallel to each other, the growth rate is the highest in the attachment direction.[43] The spherulitic growth process is a competition among different crystal growth directions, and the fastest one determines the orientation of the microcrystallites in the radial direction. Hence, the fastest growth direction of $BDH^+ClO_4^-$ is along the [10$\bar{2}$] axis, which is normal to the BDH^+ molecular plane.

But in the case of J-aggregate crystallization, where the dislocation angle α between aggregate direction *A* and the molecular plane is not 90° (α is generally <54.7°),[29] the microscopic molecular attachment direction *A* deviates from *R*. In the case of the $BDH^+ClO_4^-$ crystal, the aggregate direction deviates by 60.3° from the fastest growth direction [10$\bar{2}$]. This asymmetry does not affect the growth direction at low undercooling. Due to the low viscosity of the amorphous phase the molecules can quickly rearrange themselves into the native crystalline lattice resulting in a straight radial growth. But at high undercooling the mobility of the $BDH^+ClO_4^-$ molecules decreases, leading to a competition between the macroscopic growth along the radial direction and the microscopic attachment along the molecular aggregate directions. This introduces an asymmetry in the growth process, which we believe is the cause for both the bent growth in the BC region as well as the periodic changes of color in the banded spherulites.

A molecular mechanism for the bent growth is proposed as shown in Figure 11a. The bent growth is a result of the asymmetry between the macroscopic attachment of the molecules in the direction of the fastest growth and the microscopic attachment of the molecules in the direction *A* of the aggregate stacks. The fastest molecular attachment direction, indicated by the small arrows, is perpendicular to the molecular plane and the m_+ component. At low undercooling and low viscosity the molecules can move easily to the required position in the aggregate stacks. But at a higher viscosity, the mobility of the molecules in the amorphous phase is limited. Small attachment faults in the aggregate stacks become more likely due to the 29.7° inclination (29.7° is the dislocation α of the J-aggregate) of the aggregate direction *A* with respect to the crystalline and amorphous interface. The attachment faults are manifested as a small anticlockwise tilt of the molecular axis (from *A* to *R*) in order to maintain locally the preferred stacking angle α. Consequently, a left-handed curvature of the actual growth pattern occurs instead of the usual straight growth along *R*. Experimentally, it is not possible to decide whether the bending is from the aggregate direction to the fastest growth direction or vice versa. The first variation, illustrated in Figure 11a, is more probable based on the molecular alignment in the color period (Figure 9c).

In the case of the RC region both aggregate directions A_1 [110] and A_2 [1$\bar{1}$0] project symmetrically onto *R* in the layer plane. During growth the molecules attach symmetrically from the left and right of the *R* axis in-plane which is in good agreement with the straight pattern along the radial direction, observed in the optical and AFM measurements. But in the BC region (010) plane, both A_1 and A_2 project toward the right-handed side of *R*, whereas in the (0$\bar{1}$0) plane (not shown here), both project to the left. Due to the increasing viscosity with undercooling the expected decrease in the radius of the curvature was also observed.

It is likely that the surface roughness difference between the BC (010) and RC (201) face is a result of the surface attachment energy difference between the two faces. At the (010) face, the higher surface roughness, and the increase in film thickness accompanied by the shrinkage in the tangential direction suggest a higher growth rate in the [010] direction than in the [201] direction. At the (201) face, the higher growth rate in the

(43) Israelachvili, J. *Intermolecular and Surface Forces*; Academic Press: London, 1992; pp 67−109.

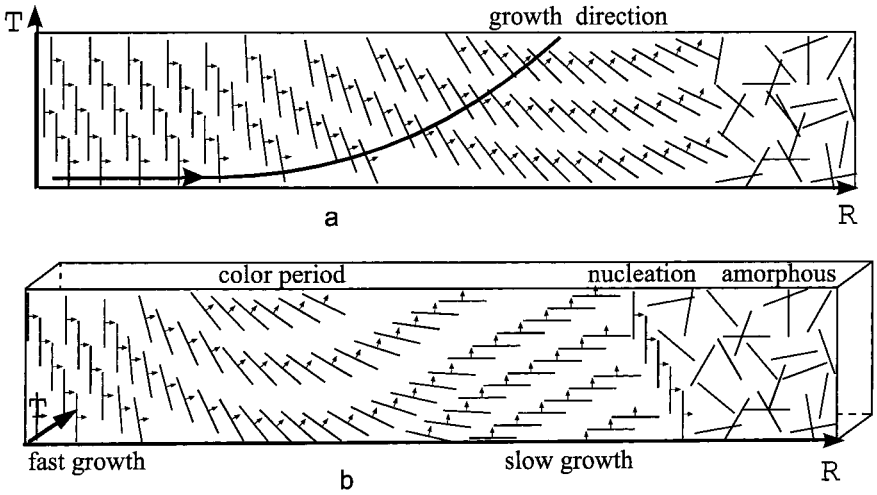

Figure 11. Illustration of the asymmetrical molecular aggregation processes. (a) Top view of the (010) face showing the bent growth due to in-plane asymmetry. (b) Side view of the (010) face showing the banded growth due to out-of-plane asymmetry. *T* is the tangential direction and *R* is the radial direction of the spherulite. For simplicity, only the exciton component m_+ was drawn, which is the bisector of the two molecular directions.

tangential direction and lower rate in the film surface normal direction produce a smoother surface formed by a 2-D network of aggregates.

Out-of-Plane Rotation of Molecular Axis in Banded Spherulites. The banded growth shares the same molecular origin as the bent growth of the BC region. As discussed above, the difference between the RC and the BC region is a 90° rotation of the crystalline lattice around *R*. Therefore, the asymmetry between *R* and *A* directions is in-plane for the BC face and out-of-plane for the RC face. When the temperature is reduced further to below 90 °C, the viscosity becomes high for the out-of-plane bent growth of the RC face. This bent growth leads to a molecular rotation around the tangential axis, which eventually rotates the crystalline lattice by 90° at the end of a color band, and changes the m_+ component from an upright in the RC tip to an in-plane position in the blue tail (Figure 9c). The rotation was derived from the dependence of the m_+ absorption energy on the angle between the transition dipole moment and the incident light beam due to the polariton theory.[12] Within one period the crystal rotates around the [010] axis, and yields the continuous exposure of different crystalline faces belonging to the (010) crystal zone.

Figure 11b illustrates the out-of-plane molecular rotation in the banded spherulite. The color period starts always with the RC face as the tip of the fan. This face has the highest radial growth rate as shown by the convex/concave boundary between two spherulites (Figure 9d). In this region, the fastest growth direction [$10\bar{2}$] is initially in-plane and parallel to the radial direction. Then the out-of-plane asymmetrical growth leads to the out-of-plane curve of the aggregate growing front. The radial growth rate slows down to a minimum when the [$10\bar{2}$] direction is rotated to the normal of the layer plane whereas the molecular plane is parallel to the layer plane. The minimum radial growth rate is apparent since the molecules attach to a growing surface that is perpendicular to the spherical front with *R* being its surface normal. Now either the crystallization keeps producing the blue region with the slowest radial growth rate or by some parasitic nucleation events it produces again the RC region with the fastest growth rate. Kinetically, the RC region wins and starts another banding as shown by our results. Unlike previous theories, this mechanism explains the molecular origin of the intermittent growth in spherulites.

This mechanism also explains the thickness variation within one color band. The fast growth of the RC region in the beginning of the period leads to high heat production and low viscosity in the immediate amorphous phase. Molecules move from the amorphous phase and attach to the interface easily, and as a result the thickness of the crystalline phase increases coupled with a decrease of thickness in the surrounding amorphous phase. When the crystalline lattice rotates upward and the film thins, a smaller amount of heat will be released due to slower crystallization rate and fewer available molecules in the amorphous phase. The temperature of the nearby amorphous phase decreases, the viscosity increases, and the thickness of the red/blue part of the band becomes smaller until the cycle starts again with the RC region. As shown by the experiments, decreasing viscosity due to lower crystallization temperature favors the asymmetrical growth pattern and leads to a smaller radius of curvature and therefore also to the decrease in the length of the period.

Our results have shown that the intermittent banding in spherulitic crystallization is a direct result of out-of-plane asymmetrical growth, caused by the deviation of aggregate directions from the radial direction of the sphere. It is not clear how the mechanism proposed here for the self-organization of the $BDH^+ClO_4^-$ layer is correlated to the banded crystallization of polymers. However, we can check the validity of previous theories developed for polymers against our results. These theories already were discussed in the Introduction.

(1) Secondary nucleation and dendritic growth[22] are chaotically determined processes and can be excluded as a reason for the color banding of the $BDH^+ClO_4^-$ due to the observed high regularity of the banding.

(2) The chiral or twisted growth in the radial direction[23] was not observed in the periodic growth of $BDH^+ClO_4^-$ films. If the molecular rotation is around the radial direction, then the color period would be observable only for light polarized in the tangential direction of the spherulite, and the wavelength would vary for the m_- component between 350 and 574 nm. In contrast to our explanation, the molecular origin for the radially twisted growth of polymers is not known. Maybe the radially and tangentially twisted growth share a similar molecular origin.

(3) The theories employing only two alternating polymorphs[24] are not valid here because of the uniform melting point in all

color regions, the continuous change of color in one band, and the constant absorption wavelengths in the tangential direction. In addition, the large amount of impurities necessary for the segregation into different polymorphic forms or the amorphous phase does not exist in the pure $BDH^+ClO_4^-$ single crystals used.

(4) The thermal effect cannot be the sole reason for the banded growth[25] even though it is likely temperature does fluctuate in one color period. The assumption of an auto-acceleration mechanism is only reasonable around the temperature of the highest growth rate, which in our case is around 135 °C (Figure 4). But no banded structure was observed above 90 °C. The color oscillation occurs at remarkably low temperatures, which would require an unreasonable temperature increase by more than 45° at the crystallizing front due to the heat of fusion.

(5) Long range flow or local stresses upon crystallization of anisotropic molecules can account for the small angle dislocation and gradual rotation of the molecular axis in highly viscous melt. Hence, the auto-orientation theory of the stress-induced rotation of the crystal lattice around the tangential direction of Schuur[26] is consistent with our observations. But the origin of the stresses, which is assumed to arise from the streaming pressure of the long polymer molecules moving in the amorphous phase to the interface, has to be rejected in the case of the $BDH^+ClO_4^-$ molecules. Our results show clearly that an inclined molecular attachment is the origin of the stresses, which is responsible for both the bent growth at low undercooling and the banded growth at high undercooling.

Before a generalization can be made based on our study, it should be pointed out that the organic dye molecules are different from polymers in several aspects. The BDH^+ molecule has a short, stiff, and rodlike molecular shape, while a polymer segment is connected with others and is in general more flexible. The attractive interactions between dye molecules are much higher than those between polymeric segments due to the high polarizability of the π-electron system. As derived from the narrow shape of the absorption bands, the degree of molecular aggregation in the $BDH^+ClO_4^-$ spherulite approaches almost 100%, a value never reached in spherulitic crystallization of polymers. In addition, the thickness of $BDH^+ClO_4^-$ layers investigated is 1 to 2 orders smaller than the layer thickness used in the polymer studies, and leads to a much faster dissipation of heat of fusion to the quartz substrate and the air.

Conclusions

Spherulitic crystallization of amorphous films of organic dye molecules was used to prepare highly ordered chromophore arrays with anisotropic absorption properties in the visible range. The color of the transparent thin films of the dye $BDH^+ClO_4^-$ was varied simply by controlling the crystallization temperature between 20 and 135 °C. The change in the optical properties is directly linked to the supramolecular architecture in the layer according to the exciton and the polariton theory. Hence, this system offers an excellent opportunity to study and explain unusual asymmetrical growth phenomena of nonchiral molecules, such as the bent growth and the banding of spherulites based on the molecular mechanisms. The structure and color correlation was established by the optical spectroscopy and microscopy, atomic force microscopy, and scanning tunneling microscopy.

The kinetics of the spherulitic growth process is in good agreement with previous experimental and theoretical studies on melt spherulitic crystallization. At low undercooling the $BDH^+ClO_4^-$ layer organizes into two different aggregate domains RC and BC, whose growth patterns are strictly radial and homogeneous. Unusual curved growth of the BC domain and banded growth of the RC domain were observed at higher undercooling. Such growth patterns are known from a variety of spherulites, especially the polymeric ones. Both types of growth patterns, the curved growth and the banding, are originated by an asymmetry between the macroscopic attachment of the molecules in the direction of the fastest growth and the microscopic attachment of the molecules in the direction of the aggregate stacks. In the case of the BC face, this asymmetry is in-plane, leading to the curved growth, whereas it is out-of-plane in the case of the RC face, leading to a rotation of the crystalline lattice around the tangential axis of the spherulite and therefore the observed banding. The banding is not a continuous oscillating process, as predicted by most theories concerning the banded growth, but an intermittent one, which is well explained by the proposed mechanism of the microscopic attachment of dye molecules to the crystalline phase.

The AFM investigations of the moving amorphous and crystalline interface in real time offered an insight into the microscopic processes of phase transitions, such as changes in the heat release, viscosity, mass transport, as well as the height and roughness of the formed crystalline layer. Although STM captured images of higher resolution, no direct observation of aggregates, crystalline lattices, or molecule direction has been accomplished.

It was shown that very thin but fully covered layers with a smooth surface can be produced by the TLA process. The tilt of the crystalline lattice can be varied widely simply by changing the TLA temperature. Such layers are especially important for the optoelectronic and electrooptical applications.

Acknowledgment. Prof. G. Mao wishes to acknowledge the donors of the Petroleum Research Fund (No. 31280-G7), administered by the American Chemical Society, and the Career Program of the National Science Foundation (CTS-9703102) for the financial support of this research. Dr. L. Daehne wishes to acknowledge the German Research Foundation and the Fond der Chemischen Industrie. The authors wish to acknowledge the Institute for Manufacturing Research (IMR) at Wayne State University (WSU) for financial support of Dr. L. Daehne's visiting stay at WSU.

JA983842V